MOEM

Modern Electronic Materials 2022; 8(4): 149–155
DOI 10.3897/j.moem.8.4.98919

Research Article

Metamaterial-based terahertz converter

Andrey V. Sabluk[1], Alexey A. Basharin[1]

1 National University of Science and Technology MISiS, 4-1 Leninsky Ave., Moscow 119049, Russian Federation

Corresponding author: Andrey V. Sabluk (sablukandrey@gmail.com)

Received 24 October 2022 ♦ **Accepted** 15 November 2022 ♦ **Published** 19 December 2022

Citation: Sabluk AV, Basharin AA (2022) Metamaterial-based terahertz converter. *Modern Electronic Materials* 8(4): 149–155. https://doi.org/10.3897/j.moem.8.4.98919

Abstract

Since the early 1980s the terahertz range (0.1 to 10 THz) attracts permanent attention of fundamental and applied science. Due to its unique properties terahertz radiation is used in a wide range of applications such as spectroscopy, non-destructive defectoscopy and security systems. The design of high-efficiency terahertz absorbers and converters is currently the main task in the development of terahertz technologies. In this work a frequency selective high-Q metamaterial is used for the fabrication of a terahertz-to-infrared converter. The converter consists of a metamaterial-based terahertz absorber coated with a micrometer-thick graphite layer that reemits the absorbed energy in the infrared range. We have carried out electrodynamic and the related thermodynamic calculations of the suggested radiation converter. Numerical simulations yield an electromagnetic radiation absorption coefficient of 99.998% and an analytically calculated converter efficiency of 93.8%. Thanks to these advanced parameters suggested terahertz converter can find it's applications in a wide range of transportation security inspection and defectoscopy tasks.

Keywords

metamaterial, terahertz radiation, infrared radiation, radiation converter, frequency selective surface

1. Introduction

The terahertz **(THz)** frequency range (0.1 to 10 THz) [1–3] is important for the science and technology for the decades to come [4]. The good promise of the terahertz spectral range for diagnostics originates from the possibility to achieve a higher spatial resolution of the produced image as compared with that for the gigahertz range and a greater penetration depth into tested objects in comparison with that for the infrared range [5]. It should be noted that THz radiation is not ionizing and penetrates into most materials, being only reflected by metals and water [6]. Security systems on the basis of the converter suggested in this work are a potential alternative to metal detectors and X-ray inspection equipment [6]. THz range detectors show good promise for the detection of latent defects, cavities, voids, cracks and foreign inclusions during materials analysis in industry [7]. However, the development of terahertz detectors faces the technical complexity associated with the fabrication of a THz sensitive matrix [8, 9].

The use of existing well-proven infrared focal plane array matrices for the processing of THz radiation converted to the IR range is a promising approach. Radiation conversion from one frequency range to another can be achieved using specially structured artificial media, i.e., metamaterials [10], consisting of multiple repeated elements in the form of metaatoms. The interaction of electromagnetic waves with these media triggers a number of phenomena that cannot be achieved using other technologies and do not occur naturally [10]. These specific phenomena include clocking, ultrastrong field localization and diffraction limit overcoming [11–13].

In recent years special attention has been drawn to metamaterials due to the possibility of the implementation on their basis of high-Q resonators operating over a wide terahertz frequency range [13–15] at different temperatures [16, 17]. Metamaterials are suitable for the fabrication of terahertz radiation sources [18], modulators [19–22] and detectors [23, 24]. Terahertz explosives detectors are used in transportation security systems [2], astronomy [25] and biomedicine [26].

The importance of converting terahertz radiation is dictated not by the necessity of reducing or increasing the frequency but rather by the practical convenience of devices and equipment operating in some technically achievable frequency range which can be adapted to operation in another range. The design of the converter includes two basic components. By analogy with detectors, the main component of the converter is the receiver, the other component being the emitter. A good signal receiver is equivalent to the perfect absorber which can be made from metamaterials [27–29].

2. Perfect absorbers

By their nature, electromagnetic wave absorbers can be divided in two categories: resonance and non-resonance ones. The absorbers of the former category are distinguished by perfect absorption in a narrow transmittance band, whereas the non-resonance absorbers are used for non-perfect wide-band absorption. To understand the reason of the choice of metamaterials as the material for the perfect absorber as component of the suggested converter, we will analyze the working principle of the resonance absorbers. The first resonance electromagnetic wave absorber was invented by the American engineer Winfield Salisbury [31] and was referred to as the Salisbury screen in honor of the inventor (Fig. 1 *a*). The working principle of the Salisbury screen is based on the phenomenon of destructive interference by analogy with antireflection coatings in optics. An electromagnetic wave incident on the Salisbury screen passes through the top transparent layer and the dielectric layer with a thickness of a quarter of the wavelength divided by the refraction index. The electromagnetic wave is then reflected from the screening bottom metallic layer where its phase undergoes a 180 deg shift which causes destructive interference resulting in electromagnetic wave extinction in the dielectric bulk [32].

3. Method of frequency selective surface

Another category of the resonance absorbers is the frequency selective surface [33]. If the frequency selective surface is hit by a wave (Fig. 1 *b*) having the frequency coincident with the resonance frequency of the frequency selective surface elements, the wave can either pass through the frequency selective surface or be reflected either completely or partially, depending on the surface topology. The frequency selective surface consists of periodic arrays of metallic elements etched on a dielectric material. From the viewpoint of electrodynamics, frequency selective surface structures can be capacitance or inductive, also referred to as spatial filters (Fig. 1 *d*). Depending on their function, the filters can either transmit or absorb radiation in a specific frequency range. A high-frequency filter (RC filter) has a surface pattern consisting of multiple tiles, its equivalent circuit being a capacitor and a resistor connected in series. A low-frequency filter (RL filter) has a grid-like surface pattern, its equivalent circuit being an inductive coil and a resistor connected in series. There is no exact applicability limit of a specific surface pattern, so in each case one should take into account the dimensions of the target structure. There can be the problem of the non-transparency of metals for electromagnetic waves with frequencies below the metal plasma frequency. Therefore when designing the top layer of the metamaterial absorber one should reduce its effective plasma frequency to below the working frequency. The plasma frequency ω_p of a metal is proportional to the square root of the charge density:

$$\omega_p = \sqrt{\frac{ne^2}{m^*\varepsilon_0}}, \tag{1}$$

where e is the electric charge, n is the charge density and m^* is the effective mass of electron. As can be seen from Eq. (1), the only method to reduce the plasma frequency is to reduce the charge density n because the other parameters (e, m^* and ε_0) are constants. The charge density can be reduced by specifically designing the metallic elements of the top layer of the frequency selective surface. The metamaterial developed in this work (Fig. 1 *c* and *e*) is a frequency selective surface absorbing at 96 GHz. The choice of this frequency is dictated by the atmospheric transparency window [34].

4. Schematic of terahertz conversion

One application of the terahertz converter suggested herein is shown in Fig. 1 *d*. A person is in the inspection zone between the 96 GHz electromagnetic source and the screen. THz radiation passes through the radiation-specific transparent media and is incident upon the terahertz converter screen. THz radiation is converted to the IR range due to heating and reemission. Reemission is achieved by coating the rear surface of the metamaterial with a thin layer of a substance whose properties are the closest to those of the absolute black body (in the case considered, this is graphite). Thus, in the converter suggested herein the incident radiation is absorbed by

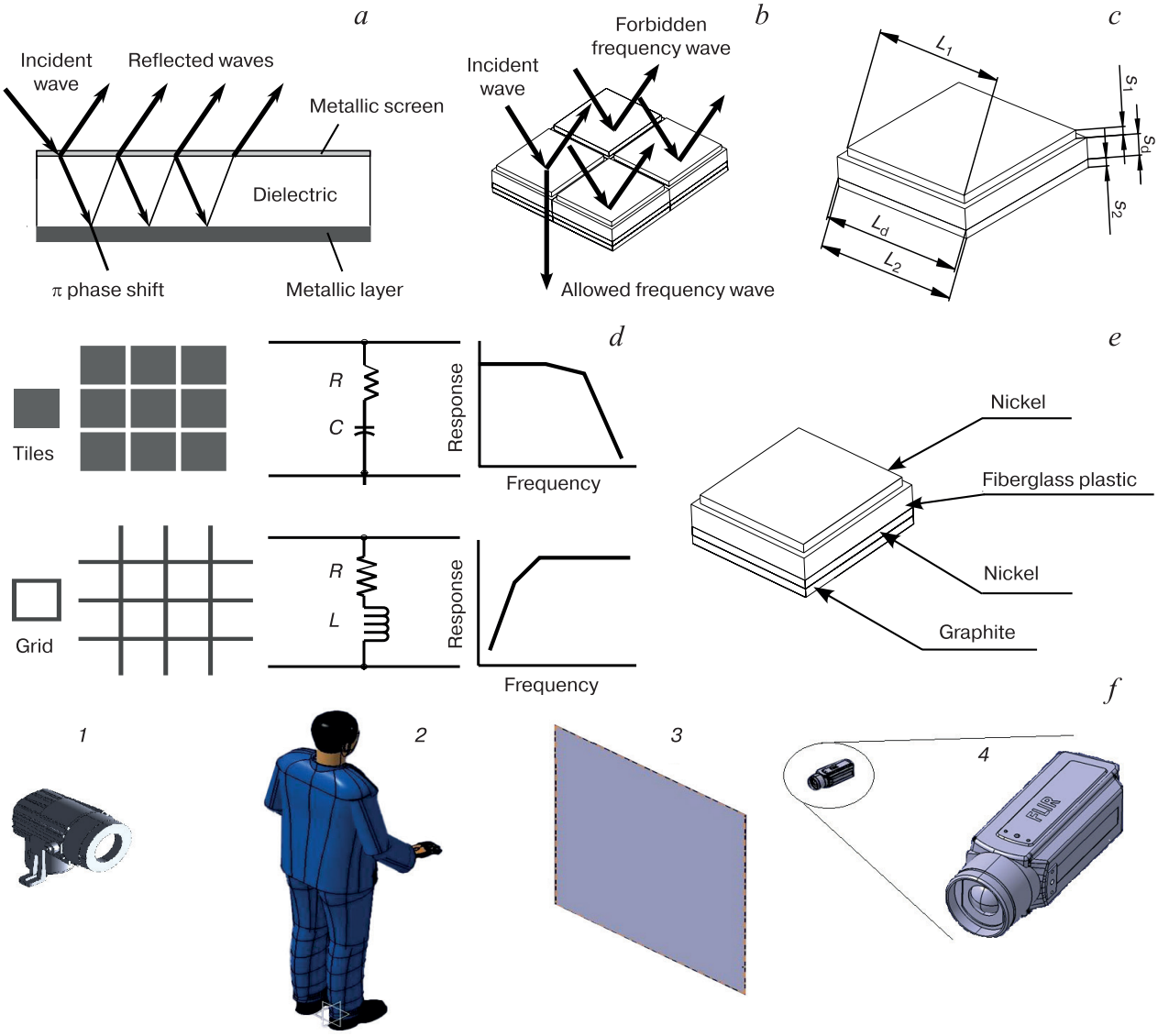

Figure 1. Physical working principles and main parameters of converter: (*a*) Salisbury screen [31] consisting of a thick screening metallic layer coated with a dielectric layer having a specially selected thickness and a thin transparent metallic screen; (*b*) frequency selective surface in the form of a 2D array of metallic elements on a dielectric substrate which reflects or absorbs electromagnetic waves at the preset frequency depending on the surface topology; (*c*) the metaatom considered herein is in the form of three superimposed layers with square cross-sections having the following dimensions: $L_1 = 0.535$ mm, $L_2 = L_d = 0.585$ mm, and thicknesses $s_1 = s_2 = 0.024$ mm and $s_d = 0.067$ mm. The overall thickness of the metamaterial is 0.115 mm; (*d*) frequency selective surfaces of two topologies and their equivalent circuits. Tiles are used in the low-frequency range, and grid is used at high frequencies; (*e*) the top and bottom conducting layers in the metaatom are nickel, the dielectric being fiberglass plastic. The bottom surface of the metamaterial is coated with graphite for radiation conversion; (*f*) example of THz converter application in security domain. The person *2* is in the inspection zone between the 96 GHz electromagnetic source *1* and the screen *3* which is the THz converter. The radiation passes through the transparent media and is incident on the terahertz converter for further conversion to IR radiation. The infrared radiation of the converter is read by the IR camera *4*

the metamaterial and the IR radiation is reemitted by the graphite layer. It is suggested to use a thermal imaging system as the IR receiver. The infrared radiation emitted by the converter is read by the IR camera. Advanced thermal imaging cameras [35] are fitted with focal plane array matrices with a resolution potentially ranging from 160×120 to 1280×720 pixels, onto which the optical system of the device focuses the thermal image of the inspected object. These matrices do not require heat removal and their spectral sensitivity is constant in a range of 1 to 14 mm. The sensitivity limit of focal plane array matrices without heat removal in commercially available models is 20 mK [35]. The spatial distribution of the THz radiation incident upon the converter is replicated by the distribution of the heat flow density reflected from the graphite layer. The thermal field of the converter is further converted to a color image on the thermal imaging system display.

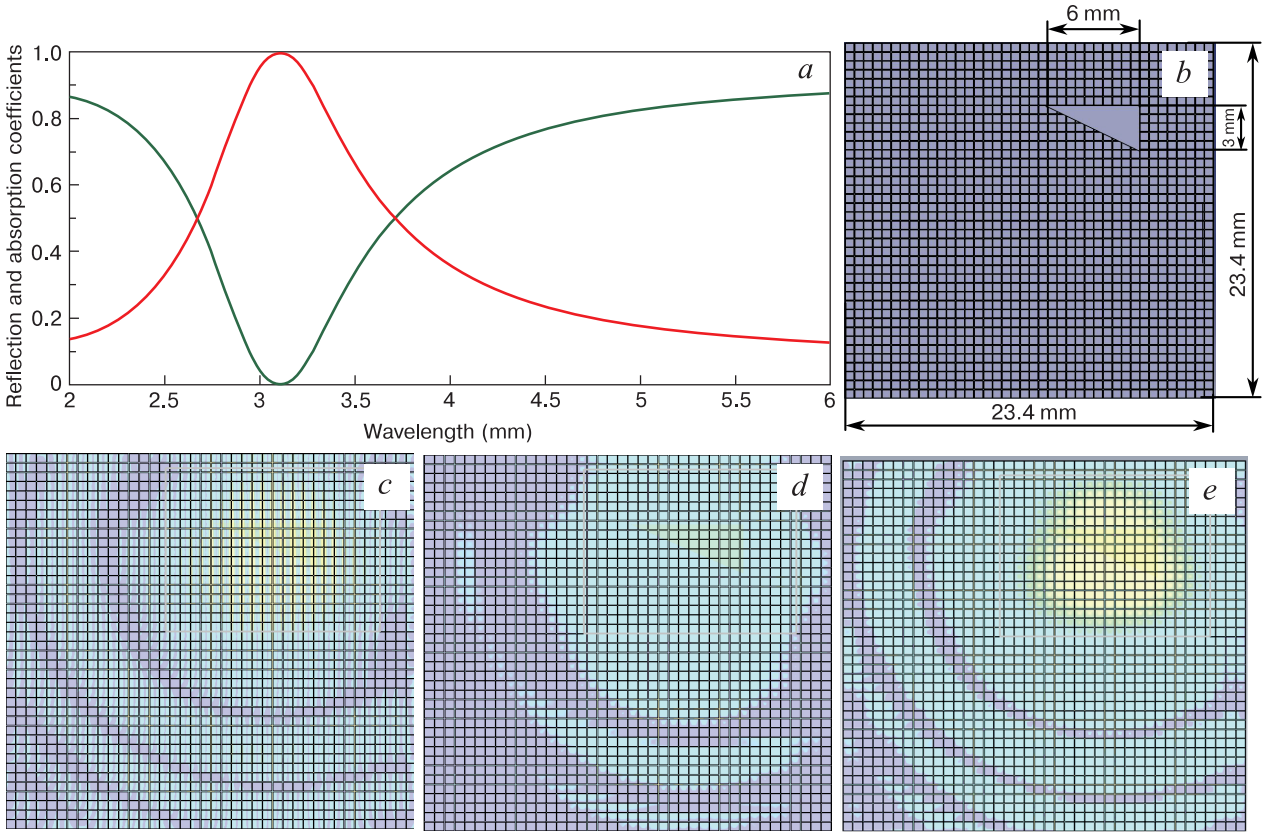

Figure 2. Results of numerical simulation of radiation absorption: (*a*) absorption coefficient (red curve) and reflection coefficient (green curve) as a function of incident radiation wavelength. Electrodynamic simulation of the newly designed metamaterial with Microwave Studio CST shows an absorption coefficient of 99.998% at 96 GHz corresponding to the wavelength $\lambda = 3.122$ mm; (*b*) example of detection of a triangular steel plate with leg sizes of 3 and 6 mm by a 23.4×23.4 mm^2 sized metasurface consisting of 40×40 cells. The steel plate is located at a 4.7 mm vertical distance and a 0.9 mm horizontal distance from the top right corner of the metasurface. The distance between the steel plate and the metasurface is 20 mm. The electromagnetic response of the metamaterial was visualized by calculation in the Microwave Studio CST electromagnetic simulation software using the finite difference time domain method (FDTD) [36]. The simulation output data were (*c*) electric field magnitude in the dielectric layer, (*d*) magnetic field magnitude and (*e*) surface current density in the metallic layer. The top right corner of the metasurface exhibits a typical diffraction pattern. The screen area in front of the object shows a bright spot corresponding to the peak magnitude of the electric and magnetic fields and the highest surface current density. As one moves away from the spot center the excitation is spread over the metasurface in the form of coaxial circles with a declining intensity

5. Electrodynamic simulation

The reflection and absorption coefficients of the material suggested in this work in the 50 to 150 GHz range were calculated with the Microwave Studio CST electrodynamic simulation software package. At 96 GHz corresponding to the wavelength $\lambda = 3.122$ mm, the absorption coefficient of the material is the highest, 99.998% (Fig. 2 *a*), which is sufficient for this absorber to be considered perfect [29]. Since we envision applications of the converter designed herein in the field of detection, it will be appropriate to consider the following example. A triangular steel plate with leg sizes of 3 and 6 mm is placed at a 20 mm distance from the metasurface (Fig. 2 *b*). The plate is shifted to the top right corner of the metasurface. The distance from the plate edge to the top edge of the metasurface is 4.7 mm and the distance from the plate edge to the right edge of the metasurface is 0.9 mm. The metasurface is a 23.4×23.4 mm^2 sized array consisting of 1600 metaatoms (Fig. 2 *b*). The results of numerical simulation using the finite difference time domain method (FDTD) [36] for the distribution of the electric and magnetic fields and the density of the surface current at 96 GHz in the metamaterial screen are shown in Fig. 2 *c*–*e*. The dimensions of the steel plate considered in this example are comparable with the wavelength of the incident radiation, causing diffraction and interference which are observed in the field and current distributions on the metamaterial screen.

6. Simulation and calculation of terahertz converter efficiency

For THz radiation conversion to infrared range the metamaterial absorber is coated with a reemitting layer having the highest degree of blackness the thickness of which should be chosen taking into account converter response time requirements. Another important condition is a uniform distribution of the reemitting material over the surface of the bottom absorber layer. Therefore the reemitting material should have the capability of being applied onto the surface in the form of a sufficiently thin layer and have good adhesion to the surface. Graphite was chosen as the reemitting material in view of the above requirements and taking into account its good adhesion to nickel [37]. For reemitting layer thickness optimization, conjugate electrodynamic and thermal calculations were carried out with Microwave Studio CST for three graphite layer thicknesses (0.2 μm, 1 μm and 2 μm), the graphite emission coefficient being accepted to be 0.97. For the simulation of a radiation converter with a 0.2 μm thick graphite layer which is two hundred times the thickness of graphene, the following thermodynamic parameters were accepted: thermal conductivity 2000 W/(m · K), heat capacity 650 J/(kg · K) and thermal expansion coefficient 3.7 m/K at t = 293.15 K [39]. For radiation converters with graphite layer thicknesses of 1 and 2 μm the graphite parameters were borrowed from the materials library of Microwave Studio CST. The emission coefficient of insulated nickel is 0.072 which is one order of magnitude lower than that of graphite, and therefore nickel emission can be ignored in heat flow density calculations. The results of all the conjugate calculations for four metamaterial cells are shown in Fig. 3 (*b–d*). For radiation converter efficiency calculation the metamaterial cell

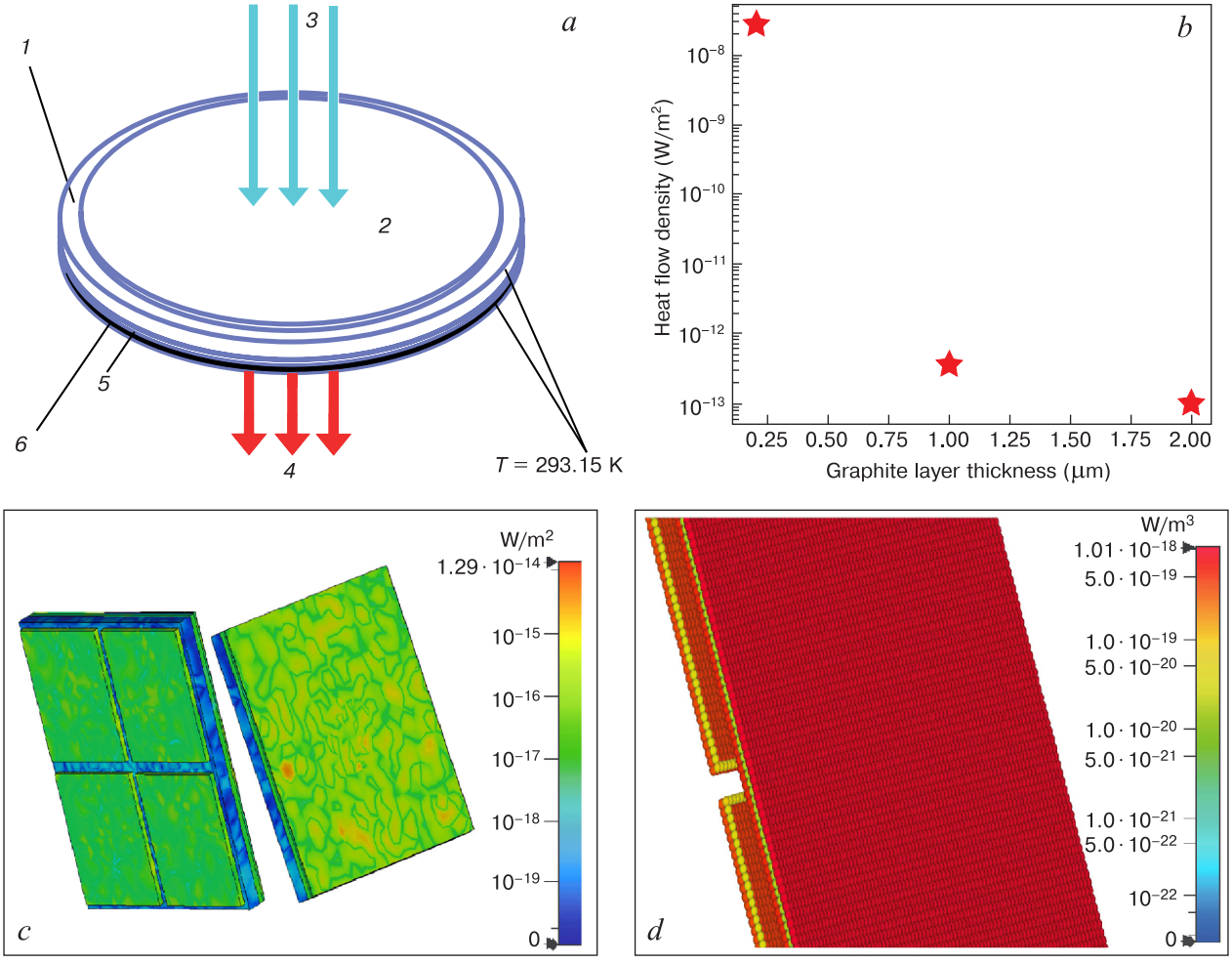

Figure 3. Radiation conversion results: (*a*) Radially symmetrical model of radiation converter cell (*1* is the fiberglass plastic, *2* is the top nickel layer of the metamaterial cell, *3* is detected THz radiation, *4* is IR radiation, *5* is the bottom nickel layer of the metamaterial cell and *6* is the graphite emitting layer). The temperature at the converter perimeter is 293.15 K. Electromagnetic and thermal calculation results obtained in the Microwave Studio CST environment. (*b*) Heat flow density of converted THz radiation for three graphite layer thicknesses (0.2, 1 and 2 μm). The best result was obtained for the 0.2 μm thick graphite layer as it delivers the highest heat flow density and hence the greatest image contrast on the focal plane array matrix of the thermal imaging system. Images of (*c*) surface heat flow density and (*d*) bulk heat flow density suggest that it is the emitting layer in the radiation converter that provides for heat emission

was adapted to a radially symmetrical model for thermal conductivity problem solution convenience (Fig. 3 *a*). In accordance with the numerical simulation conditions, the radiation converter cell is in vacuum and its symmetry axis is collinear with the THz radiation incident upon the cell surface. For a cylindrical cell the area and thickness of the elements were the same as those for the original cell. The diameter of the bottom metamaterial cell part and the dielectric layer was 0.66 mm, the top cell diameter being 0.6 mm.

The radiation converter efficiency was calculated as the ratio of the heat radiation energy E_{out} to the incident terahertz radiation energy E_{in}. The IR radiation energy E_{out} was evaluated with CST using conjugate calculation. The terahertz radiation pulse duration was 3 s. The boundary conditions were as follows: the converter temperature was accepted to be constant and equal to 293.15 K, the maximum energy flow density of incident radiation P was accepted to be 10 W/m^2 and the thermal energy accumulation time by the metamaterial was chosen to be $t_{mm} = 20$ seconds due to the relatively low thermal conductivity and significant thickness of the dielectric. The converter efficiency η in percents was calculated using the following equations:

$$\eta = \frac{E_{out}}{E_{in}} \times 100\%;$$

$$E_{in} = \int_0^{t_{imp}} dt \int_0^R P(t,r)\, 2\pi r dr;$$

$$E_{out} = \int_0^{t_{mm}} dt \int_0^R \varepsilon\sigma\left(T^4 - T_0^4\right) 2\pi r dr,$$

where ε is the radiation coefficient, σ is the Stefan–Boltzmann constant, $P(t,r)$ is the maximum energy flow density of incident radiation, t_{mm} is the thermal energy accumulation time by the metamaterial cell and t_{imp} is the THz radiation pulse duration. The best converter efficiency reaching 93.8% was achieved for the minimum emitting layer thickness of 0.2 mm.

7. Conclusion

A model of a metamaterial-based terahertz converter was suggested. The working principle of the converter is based on the absorption of THz radiation by a resonance metamaterial absorber, converter heating and heat reemission by a thin graphite layer. The emitted IR radiation can be detected by the focal plane array matrix of a thermal imaging system. The metamaterial absorber is designed for operation at 96 GHz at which the absorption coefficient of the converter is 99.998%. The converter has low heat capacity and therefore high sensitivity. The best converter efficiency as calculated in the course of numerical simulation was 93.8%. This converter can find application in THz radiation visualization for defect diagnostics in industry and in security domain.

Acknowledgment

The Authors are grateful to N.A. Maleeva for her mentoring in academic writing. The work was carried out with financial support from the Ministry of Science and Higher Education of the Russian Federation within State Assignment for the National University of Science and Technology MISiS (Assignment Code 0718-2020-0025).

References

1. Kulchitsky N.A., Naumov A.V., Startsev V.V., Demyanenko M.A. Detection in the terahertz range. Part 1. *Photonics Russia*. 2021; 15(1): 52–69. (In Russ.). https://doi.org/10.22184/1993-7296.FRos.2021.15.1.52.68
2. Song H.D., Nagatsuma T., eds. Handbook of terahertz technologies: devices and applications. 1st ed. NY, USA: Jenny Stanford Publishing; 2015. 612 p. https://doi.org/10.1201/b18381
3. Peiponen K.E., Zeitler J.A., Kuwata-Gonokami M., eds. Terahertz spectroscopy and imaging. Berlin, Heidelberg: Springer-Verlag; 2013. 644 p. https://doi.org/10.1007/978-3-642-29564-5
4. Usanov D.D., Romanova N.V., Saldina D.D. Prospects and trends in the development of terahertz technologies: patent landscape. *The Economics of Science*. 2017; 3(3): 189–202. https://doi.org/10.22394/2410-132X-2017-3-3-189-202
5. Akhmanov A.S., Angeluts A.A., Balakin A.V., Nazarov M.M., Ozheredov I.A., Sapozhnikov D.A., Sokolov V.I., Khaidukov E.V., Shkurinov A.P., Panchenko V.Ya. Terahertz optoelectronics and its applications. Moscow: Interkontakt Nauka; 2014. 785 p. (In Russ.)
6. Zimdars D., White J., Stuck G., Sucha G., Fichter G., Williamson S.L. Time domain terahertz imaging of threats in luggage and personnel. *International Journal of High Speed Electronics and Systems*. 2007; 17(2): 271–287. https://doi.org/10.1142/S0129156407004497
7. Carranza I.E., Grant J., Gough J., Cumming D.R.S. Metamaterial-based terahertz imaging. *IEEE Transactions on Terahertz Science and Technology*. 2015; 5(6): 892–901. https://doi.org/10.1109/TTHZ.2015.2463673
8. Liu D., Gaucher B., Pfeiffer U., Grzyb J., eds. Advanced millimeter-wave technologies: antennas, packaging and circuits. John Wiley & Sons, Ltd; 2009. 769 p. https://doi.org/10.1002/9780470742969
9. Sakai K., ed. Terahertz optoelectronics Springer Berlin, Heidelberg; 2005. 389 p. https://doi.org/10.1007/b80319
10. Ali A., Mitra A., Aïssa B. Metamaterials and metasurfaces: A review from the perspectives of materials, mechanisms and advanced

metadevices. *Nanomaterials*. 2022; 12(6): 1027–1059. https://doi.org/10.3390/nano12061027

11. Pendry J.B. Negative refraction makes a perfect lens. *Physical Review Letters*. 2000; 85(18): 3966–3969. https://doi.org/10.1103/PhysRevLett.85.3966
12. Fedotov V.A., Rose M., Prosvirnin S.L., Papasimakis N., Zheludev N.I. Sharp trapped-mode resonances in planar metamaterials with a broken structural symmetry. *Physical Review Letters*. 2007; 99(14): 147401–147406. https://doi.org/10.1103/PhysRevLett.99.147401
13. Al-badri K. Very high Q-factor based on G-shaped resonator type metamaterial absorber. *Ibn AL-Haitham Journal for Pure and Applied Science. 2017 (IHSCICONF)*. 2018: 160–168. https://doi.org/10.30526/2017.IHSCICONF.1788
14. Savinov V., Fedotov V.A., Anlage S.M., de Groot P.A.J., Zheludev N.I. Modulating sub-THz radiation with current in superconducting metamaterial. *Physical Review Letters*. 2012; 109(24): 243904–243909. https://doi.org/10.1103/PhysRevLett.109.243904
15. Al-Naib I., Yang Y., Dignam M.M., Zhang W., Singh R. Ultra-high Q even eigenmode resonance in terahertz metamaterials. *Applied Physics Letters*. 2015; 106(1): 011102–011109. https://doi.org/10.1063/1.4905478
16. Vahala K.J. Optical microcavities. *Nature*. 2003; 424(6950): 839–846. https://doi.org/10.1038/nature01939
17. Savinov V., Tsiatmas A., Buckingham A.R., Fedotov V.A., de Groot P.A.J., Zheludev N.I. Flux exclusion superconducting quantum metamaterial. *Scientific Reports*. 2012; 2(1): 450–456. https://doi.org/10.1038/srep00450
18. Liu D., Yan Y. Investigations on a dual-frequency operation terahertz gyrotron. In: *OSA Technical Digest (online). The 8th Inter. symp. on ultrafast phenomena and terahertz waves. Chongqing, China. October 10–12, 2016*. Washington, DC, USA: Optica Publishing Group; 2016. https://doi.org/10.1364/ISUPTW.2016.IW2A.4
19. Savinov V., Fedotov V.A., Anlage S.M., de Groot P.A.J., Zheludev N.I. Modulating sub-THz radiation with current in superconducting metamaterial. *Physical Review Letters*. 2012; 109(24): 243904–243909. https://doi.org/10.1103/PhysRevLett.109.243904
20. Chen H., Padilla W.J., Zide O., Gossard A.C., Taylor A.J., Averitt R.D. Active terahertz metamaterial devices. *Nature*. 2006; 444: 597–600. https://doi.org/10.1038/nature05343
21. Srivastava Y.K., Manjappa M., Cong L., Krishnamoorthy H.N.S., Savinov V., Pitchappa P., Singh R. A superconducting dual-channel photonic switch. *Advanced Materials*. 2018; 30(29): e1801257. https://doi.org/10.1002/adma.201801257
22. Srivastava Y.K., Manjappa M., Krishnamoorthy N.S., Singh R. Accessing the high-Qdark plasmonic fano resonances in superconductor metasurfaces. *Advanced Optical Materials*. 2016; 4(11): 1875–1881. https://doi.org/10.1002/adom.201600354
23. Wang Y., Han Z., Du Y., Qin J. Ultrasensitive terahertz sensing with high-Q toroidal dipole resonance governed by bound states in the continuum in all-dielectric metasurface. *Nanophotonics*. 2021; 10(4): 1295–1307. https://doi.org/10.1515/nanoph-2020-0582
24. Strikwerda A., Tao H., Kadlec E.A., Fan K., Padilla W., Zhang X., Shaner E.A., Averitt R. Metamaterial based terahertz detector. In: OSA Technical Digest (online). *Conf. on lasers and electro-optics 2011 (CLEO 2011). May 1–6, 2011. Baltimore, MD, USA*. Washington, DC, USA: Optica Publishing Group; 2011. https://doi.org/10.1364/QELS.2011.QTuD6
25. Feldman Y., Puzenko A., Ishai P.B., Caduff A., Agranat A.J. Human skin as arrays of helical antennas in the millimeter and submillimeter wave range. *Physical Review Letters*. 2008; 100(12): 128102–128107. https://doi.org/10.1103/PhysRevLett.100.128102
26. Park G.-S., Kim Y.H., Han H., Han J.K., Ahn J., Son J.-H., Park W.-Y., Jeong Y.U., eds. Convergence of terahertz sciences in biomedical systems. Springer Dordrecht; 2012. 435 p.
27. Alves F., Pimental L., Grbovic D., Karunasiri G. MEMS terahertz-to-infrared band converter using frequency selective planar metamaterial. *Scientific Reports*. 2018; 8(1): 12466–12480. https://doi.org/10.1038/s41598-018-30858-z
28. Bilgin H., Zahertar S., Sadeghzadeh S., Yalcinkaya A.D., Torun H. A MEMS-based terahertz detector with metamaterialbased absorber and optical interferometric readout. *Sensors and Actuators A: Physical*. 2016; 244: 292–298. https://doi.org/10.1016/j.sna.2016.04.021
29. Landy N.I., Sajuyigbe S., Mock J.J., Smith D.R., Padilla W.J. Perfect metamaterial absorber. Physical Review Letters. 2008; 100(20): 207402–207409. https://doi.org/10.1103/PhysRevLett.100.207402
30. Askerzade I. Physical properties of unconventional superconductors. In: *Unconventional superconductors. Springer series in materials science*. Berlin, Heidelberg: Springer; 2012. Vol. 153. P. 1–26. https://doi.org/10.1007/978-3-642-22652-6_1
31. Tao H., Bingham C.M., Strikwerda A.C., Pilon D., Shrekenhamer D., Landy N.I., Fan K., Zhang X., Padilla W.J., Averitt R.D. Highly flexible wide angle of incidence terahertz metamaterial absorber: design, fabrication, and characterization. *Physical Review B. Condensed Matter*. 2008; 78: 241103 (R). https://doi.org/10.1103/PHYSREVB.78.241103
32. Munk B.A. Frequency selective surfaces: Theory and design. Wiley; 2000. 440 p.
33. Kas'yanov A.O., Obukhovets V.A. Frequency-selective surfaces. Main Applications. *Radioengineering*. 2005; (9(100)): 4–12. (In Russ.)
34. Voytsehovskiy A.V., Nesmelov S.N., Kulchitskiy N.A., Melnikov A.A., Maltsev P.P. Detection in terahertz range. *Nano- and Microsystems Technology*. 2012; (2(139)): 28–35. (In Russ.)
35. Pocket practical guide to thermography. Testo AG; 2018. 56 p. (In Russ.). https://domikelectrica.ru/wp-content/uploads/2018/11/Testo_Prakticheskoe_rukovodstvo_po_termografii.pdf
36. Hao Y., Mittra R. FDTD modeling of metamaterials: Theory and applications. Boston; London: Artech House Publishers; 2009. 33 p.
37. Adamchuk Yu.O., Boguslavskii Yu.O., Boguslavskii L.Z., Sinchuk A.V. Deposition of carbon nanostructured coatings on metal surfaces by electric discharge method in a hydrocarbon medium. *Elektronnaya obrabotka materialov = Electronic Processing of Materials*. 2017; 53(6): 1–7. (In Russ.). https://doi.org/10.5281/zenodo.1051302
38. Mayanov E.P., Elizarov P.G., Beilina N.Yu., Bubnenkov I.A., Kolesnikov S.A., Protsenko A.N., Firsova T.D., eds. The research institute of structural materials based on graphite is 55 years old. Moscow: Nauchnye tekhnologii; 2015. 246 p. (In Russ.)
39. Brazhe R.A., Kochaev A.I., Meftakhutdinov R.M. Graphenes and their physical properties. Ulyanovsk: UlGTU; 2016. 139 p. (In Russ.)